ON THE COLLAPSING BEHAVIOR OF CAVITATION BUBBLE CLUSTERS

Akihisa Konno
National Maritime Research Institute
Tokyo 181–0004, Japan

Hajime Yamaguchi
The University of Tokyo
Tokyo 113–8656, Japan

Hiroharu Kato
Toyo University
Saitama, 350–8585, Japan

Masatsugu Maeda
The University of Tokyo
Tokyo 113–8656, Japan

Abstract

The present paper reports observation results of collapsing cavity bubbles on a two-dimensional foil section by a high-speed video camera, together with impulsive force measurement. Results of numerical simulations of the behavior of bubble cluster corresponding to the above condition are also shown. With these materials the authors discuss the mechanism of generation of the impulsive force due to cavitation collapse.

1 Introduction

Cavitation sometimes gives detrimental effects on fluid machinery such as pumps, water turbines and marine propellers. These effects are erosion, severe vibration and noise, and are mainly caused by cavity bubbles collapsing very violently at the final stage of its life. The maximum pressure generated by this collapse is estimated more than a few hundred MPa in very short time of less than a millisecond. Because of such a high pressure in very short time, it is difficult to examine especially in an actual flow field.

So far, theoretical and numerical schemes were chiefly used to simulate collapse or vibration of bubble clusters (D'Agostino and Brennen (1989), Kumar and Brennen (1993), Wang and Brennen (1994), Wang and Brennen (1995), Kameda and Matsumoto (1996)). However, results of these simulations were rarely verified by experiments. Development of experimental technique to investigate the collapsing stage of the bubble cluster is of vital requirement to understand and prevent the harmful effects of cavitation.

The present paper reports observation results of collapsing cavity bubbles on a foil section by a high-speed video camera, together with impulsive force measurement. The authors also tried to simulate the behavior of bubbles numerically.

2 Experimental Procedure

Impulsive force was measured by sensors designed and manufactured by the authors, with PVDF (polyvinylidene fluoride) piezoelectric polymer film (Figure 1). The sensors could only measure impulsive force, not pressure, because the area of impulsive pressure acting on the sensor was not known. A PVDF film of 110 μm in thickness was pasted on a 10 mm cubic brass block, and covered by thin polyimide tape for water insulation. The size of sensitive area was 3 mm $\times$ 3 mm. This impulsive force sensor had a high resonance frequency (about 10 MHz) with relatively high output, so that it was suitable for the present purpose.

Four sensors were embedded on a 2D NACA 0015 section (Chord: 150 mm, Span: 150 mm) as shown in Figure 2. Before this experiment we made a paint test with the same foil, and decided the position of sensors where many erosion pits (or more precisely, pits where the paint came off) had been observed. We observed the phenomena mainly above Sensor 3 or 4 because these were closer to the window, so that we had a better view with less obstructing bubbles.

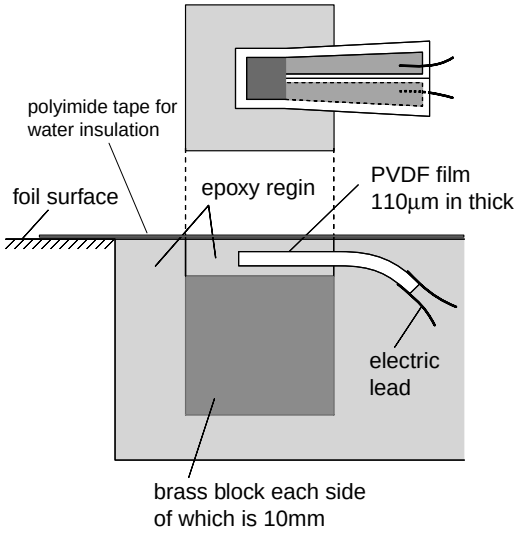

Figure 1: Impulsive force sensor

Figure 2 also shows facilities for the present experiments. A transient converter (TCFL-8000SR by Riken Denshi Co. Ltd.) was used to record the output voltage of the sensor. This converter holds the transient amplitude when it exceeds the predefined threshold voltage, and at the same time it produces trigger output. In the present experiment this output was connected to a high-speed video controller to hold images.

Observation was made by a high-speed video camera (FASTCAM-ultima(R) by PHOTRON Limited) mostly at a speed of 40,500 frames per second. Size of imaging area depends on the recording speed and 64×64 pixels in case of $40,500$ fps. Images are stored as a sequence of digital monochrome pictures in which depth of gray-scale is 8bit (256 levels), and these can be recorded to a normal video cassette recorder or into the computer storage. The video controller has a trigger input to hold the current sequences of images recorded, and by triggering it when an impulsive force had been measured by an appropriate sensor, we took sequential pictures of cavity bubbles before and after the collapse of them, which corresponded to the impulsive force.

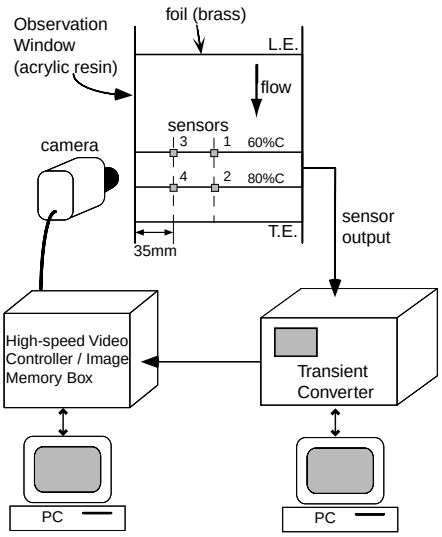

Figure 2: Sensor embedded positions and experimental facilities

Experiments were conducted in the Marine Propeller Cavitation Tunnel of the University of Tokyo fitted with a $150\,\text{mm} \times 600\,\text{mm}$ rectangular test section. The angle of incidence could be accurately varied using a digital micro-protractor. Free-stream velocity was measured with a laser-Doppler velocimeter and the tunnel static pressure was obtained from a pressure transducer. Experimental conditions were as follows: angle of attack was 8 degrees; main flow velocity $8\,\text{m/sec}$; cavitation number 1.5.

3 Experimental Results and Discussions

Figure 3 shows a series of pictures at cavity collapsing stage with impulsive force signal on sensor 3. Frame (0) corresponds to the time of trigger signal. It should be noted that both the frames of negative numbers (before the trigger)

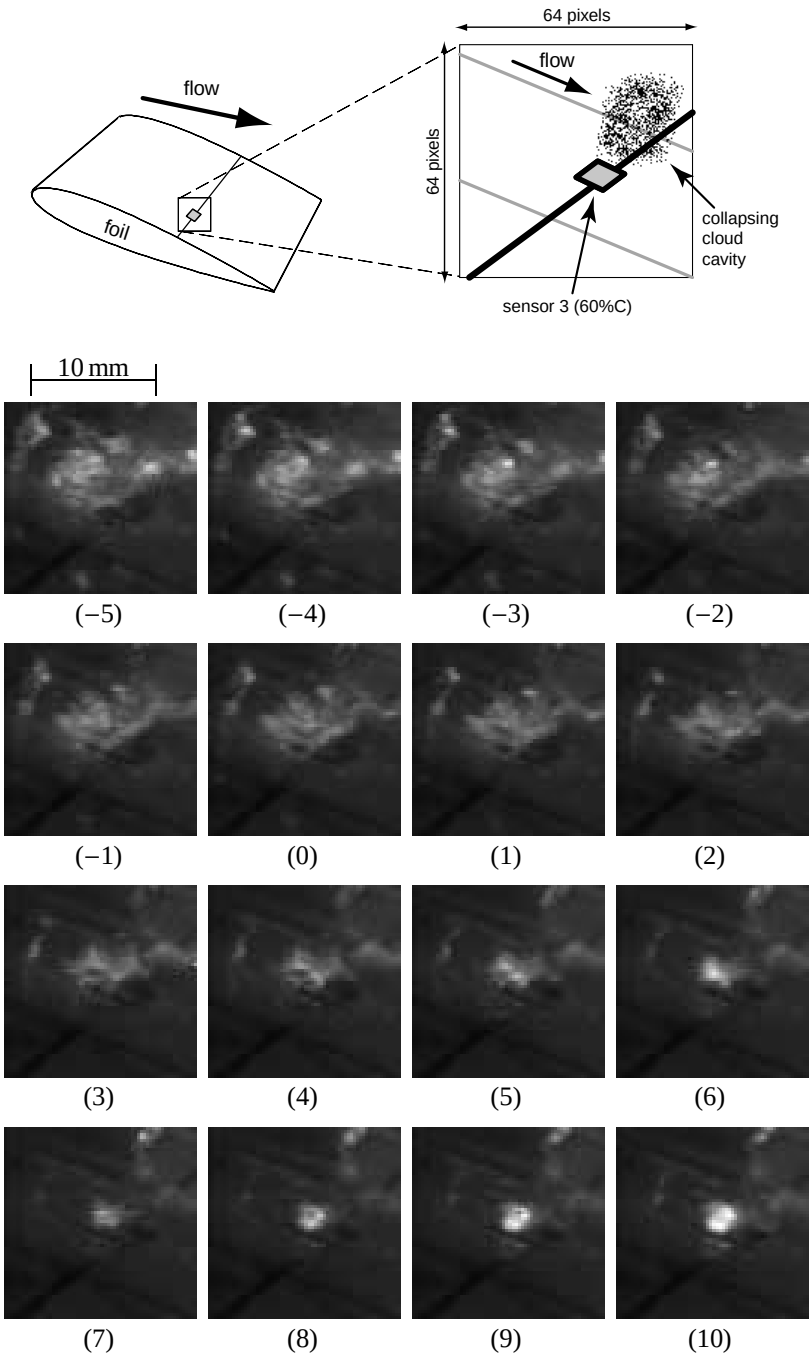

Figure 3: An example of sequence of bird's-eye pictures by high-speed video camera at the time when impulsive force was measured

and positive numbers (after the trigger) could be observed through the memory of the video system. Corresponding impulsive force signal is shown in Figure 4. 50 cases of such images and corresponding impulsive forces were recorded and analyzed.

From these observations with impulsive force measurements, the following was obtained.

1. The impulsive force always occurred with the collapse of cloud cavity and was never observed without cloud cavity collapse.
2. A second peak of impulsive force was observed in some cases, which corresponded to the second collapse of

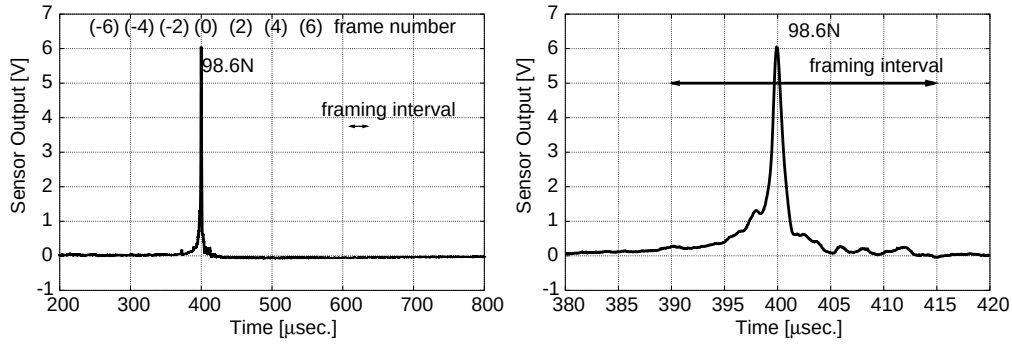

Figure 4: Sensor output voltage corresponding to Figure 3

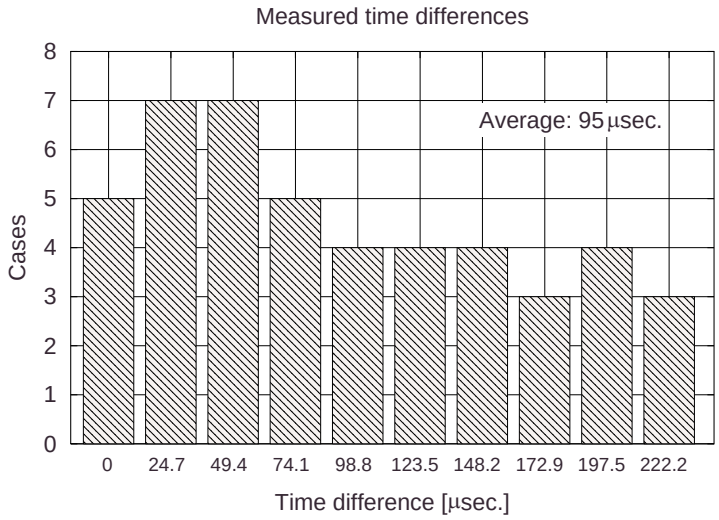

Figure 5: Number of measured cases of time difference between cavity collapses and occurrences of impulsive forces

cavity after its rebound. The same phenomena were reported by Sato and Ogawa (1995).

3. The frame interval of the video was about 24.7 μsec. Whereas the duration of impulsive force was only about 5 μsec. So although the frame rate is very high, it seems still insufficient for the observation of collapsing stage. Frame size (64×64 pixels) is also insufficient for the precise observation. It is required of such experiments to improve both frame rate and size of high-speed imaging systems.
4. Duration of the collapse was the order of 10 to 100 μsec., which is by far slower than that of the impulsive force that was around 5 μsec. as mentioned above.
5. In most cases the peak of the impulsive force was observed several frames (25 μsec. to 220 μsec.) before the cloud cavity appeared to be minimum in its volume. Observed time difference is shown in Figure 5 and these average is 95 μsec. Not observed was the case that the collapse preceded the impulsive force. The same phenomenon seems to be seen (but is not mentioned) in Fig.13(a) of Sato and Ogawa (1995).

The last item is important to investigate the mechanism of impulsive pressure generation. Considering the results above, the scenario of the collapse of cavitation bubble clusters may be the following. (Illustrated with Figure 6.)

In the bubble cluster, propagation speed of pressure fluctuation (sound speed) is slower than that in circumference. So it causes the shock wave propagation into the inside when the surrounding pressure increases. On the front of the shock wave there is high-pressure region and bubbles collapse there. After the shock wave passes, there comes low-pressure region so that the collapsed bubbles rebound rapidly.

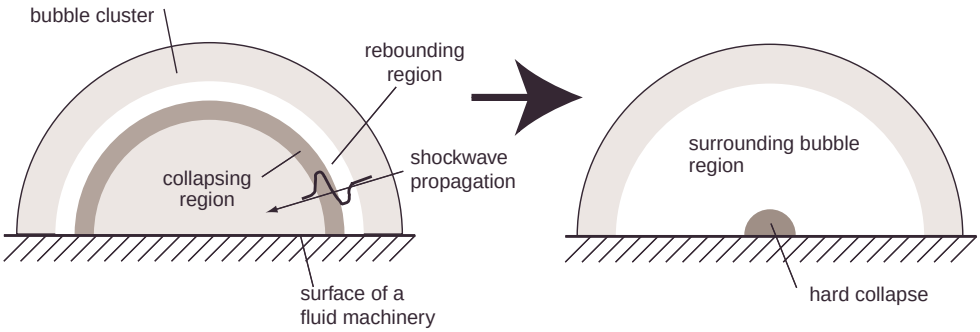

Figure 6: Illustration of cavity collapse by shock wave propagation

When this shock wave reaches and focuses at the center of the bubble cluster, it causes bubbles collapse violently and produces strong impulsive force. However, the collapsing region is surrounded by rebounded bubbles, the bubble cluster looks as if it were not yet collapsed completely.

Similar phenomenon was numerically simulated by Shimada et al. (1999), Shimada et al. (2000).

4 Numerical Simulation of the Interactions of Bubbles

The authors also tried simulating the behavior of bubbles numerically. This simulation was based on the research by Takahira (Takahira et al. (1994)). The characteristics of his work is that he considered the vibration of each bubble in the bubble cluster individually, and thus did not use so called "bubble two-phase flow modeling" which represents the bubble-liquid mixture as single-phase compressible fluid with special compression/swelling behavior. The reason why Takahira's research work was used in this paper was that the authors would like to use the most primitive modeling of the nature and to see the behavior of each bubble.

In Takahira's (and our) simulation the following conditions were assumed.

1. In bubbles there are vapor and non-condensation gas. Vapor pressure is constant, and non-condensation gas obeys polytropic change.
2. Density of gas is smaller, enough to be neglected, than that of liquid.
3. Liquid is compressible. So the fluctuation between two bubbles transmits at a speed of sound.
4. Velocity of liquid far from bubbles is zero.
5. Viscosity of surrounding liquid is ignored except for the motion of bubble wall.
6. Bubbles are always spherical.
7. Transitional motion of bubbles is ignored. Thus this simulation cannot express the expansion/shrinkage of the size of the bubble cluster.

From the above conditions, the following equation was obtained.

$$\left\{1-(\Lambda+1)\frac{\dot{R}_{I0}(t)}{a_\infty}\right\}R_{I0}(t)\ddot{R}_{I0}(t)+\frac{3}{2}\left\{1-\left(\Lambda+\frac{1}{3}\right)\frac{\dot{R}_{I0}(t)}{a_\infty}\right\}\dot{R}_{I0}^2(t)$$
$$+\sum_{J-1,\ J\neq I}^{N}\frac{R_{J0}(\zeta_{JI})}{L_{IJ}}\left\{R_{J0}(\zeta_{JI})\ddot{R}_{J0}(\zeta_{JI})+2\dot{R}_{J0}^2(\zeta_{JI})\right\}$$
$$=\left\{1+(1+\Lambda)\frac{\dot{R}_{I0}(t)}{a_\infty}\right\}\left\{h_{Iw}(t)+\dot{\Phi}(t)\right\}+\frac{R_{I0}(t)}{a_\infty}\left\{\dot{h}_{Iw}(t)+\ddot{\Phi}(t)\right\}.$$

Here I and J: bubble indices, R_{I0}: bubble radius, a_∞: sound speed in liquid, L_{IJ}: distance between bubble I and J, h_{Iw}: enthalpy at bubble wall and Φ: velocity potential of the far field. $\zeta_{JI}=t-\{L_{JI}-R_{J0}(\zeta_{JI})\}/a_\infty$ represents the duration

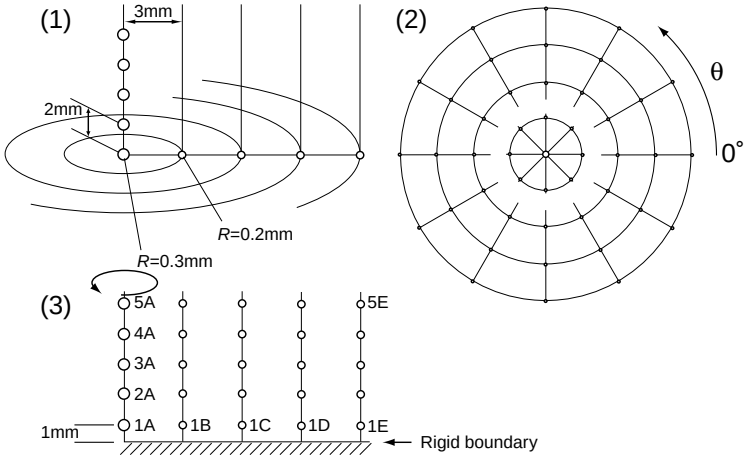

Figure 7: Initial bubble distribution for the simulation

of pressure propagation from bubble J to bubble I, i.e. delay of mutual interaction. The third term of the left hand side represents mutual interference of bubbles so that it disappears if the distances between bubbles are far enough ($L_{IJ} \to \infty$). In this case the equation comes down to that of single bubble obtained by Prosperetti and Lezzi (1986). Λ is an arbitrary parameter between 0 and 1 and it was also introduced by Prosperetti and Lezzi (1986).

The authors wrote a simulation program to solve the above ordinary differential equation for each bubble by traditional Runge-Kutta method. As an initial condition of the simulation, bubbles were placed near a wall and axis-symmetrical to the normal vector of the wall (Figure 7). We could only simulate the case that the distance between bubbles was far enough, because we assumed linear mutual interaction between each bubbles. So that void ratio of the bubble cluster was far smaller than that of real cloud cavitation (Figure 9): Stutz and Reboud measured the void fraction of sheet cavitation shedding vapor cloud and the void fraction at the end of the sheet cavitation was around 10% (Stutz and Reboud (1997a), Stutz and Reboud (1997b), Stutz and Reboud (2000)).

Time variation of surrounding pressure was determined from the pressure distribution of cavitating NACA0015 hydrofoil to correspond to the experimental condition. That pressure distribution was calculated by Yamaguchi's program (Yamaguchi and Kato (1983)).

5 Results of the Simulation and Discussions

Figure 8 shows results of the simulation. Indices of bubbles in this and the next figures correspond to that of Figure 7. The following results were obtained.

1. Bubbles collapsed and rebounded from outside to inside. This corresponds to the observed behavior of the cloud cavity in the experiments discussed in the previous section.
2. Bubble 1A (on axis, near the rigid boundary) collapsed later than the others, shrunk the smallest and produced the highest pressure.
3. At the moment the bubble 1A collapsed, the surrounding bubbles started rebounding. This results correspond qualitatively to the experimental results described in the former part of this paper.
4. However, that collapse was after the void ratio of the bubble cluster became minimum, as in Figure 9. And vibrations of bubbles were too fast. These results do not match up to the experimental results.
5. In this simulation the distances between bubbles had to be far enough to be calculated, or the results diverged. To simulate more realistic condition—denser bubble distribution—nonlinear mutual interference should be considered.

Figure 10 compares the motion of single bubble, twin bubbles and bubble clusters (1A of the previous result). It shows that the denser bubbles placed, the slower bubbles collapsed and the higher the pressure produced. This suggests that the mismatch mentioned above might have been reduced if the denser condition could be calculated.

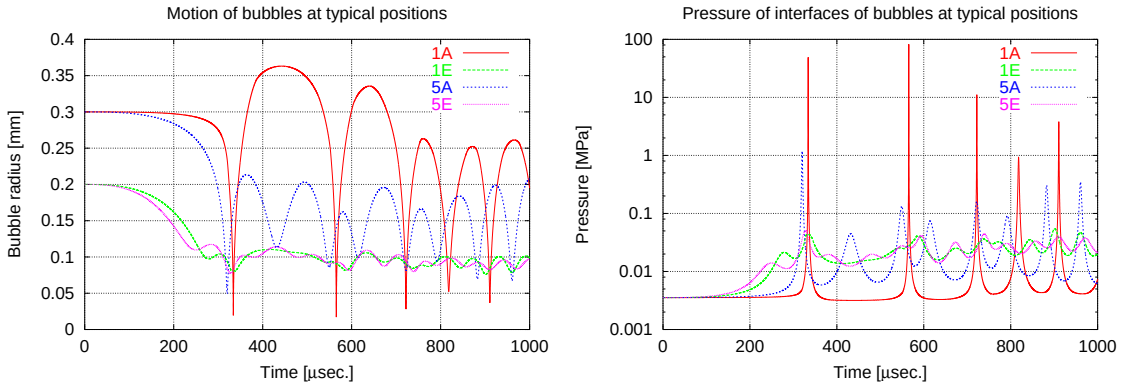

Figure 8: Time variation of bubble radii and pressures on the bubble wall

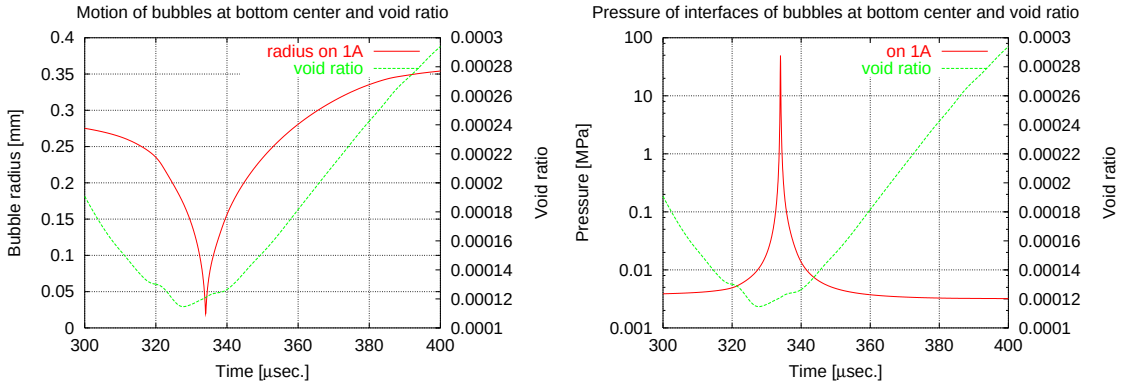

Figure 9: Time variation of radius and pressure of bubble 1A compared with void ratio

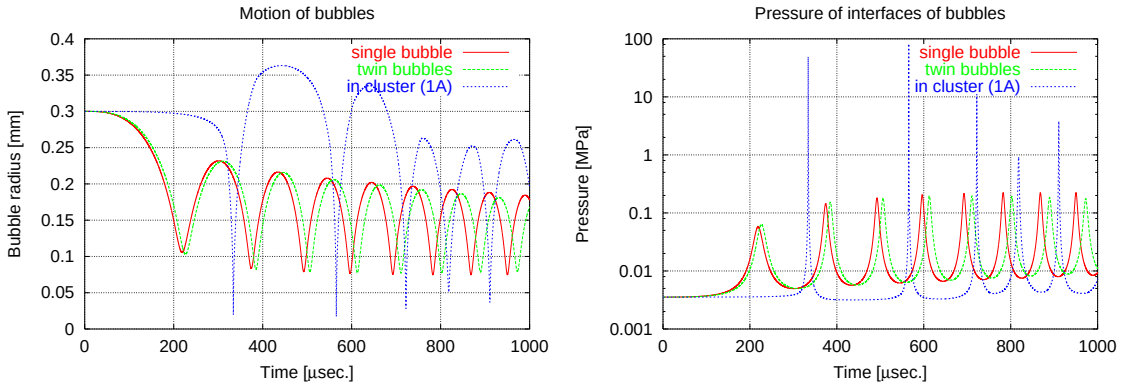

Figure 10: Time variation of bubble radii and pressures on the bubble wall: comparison with single and twin bubbles

6 Conclusions

The appearance of cavitation bubbles near the bubble collapsing stage was investigated on the foil section with a high-speed video camera that was triggered by the signal of impulsive force sensor. The minimum frame interval of the high-speed video camera was about 24.7 μsec., whereas the duration of impulsive force was only about 5 μsec. So it

seems still insufficient for the observation of collapsing stage. The impulsive force always occurred with the collapse of cloud cavity and was never observed without cloud cavity collapse, and in most cases the impulsive force peak was observed several frames (95 μsec. in average) before the cloud cavity appeared to be minimum in its volume. As a reason for this phenomenon, the shock wave propagation in the bubble cluster into its center was discussed. This new finding should be verified more experimentally as well as theoretically.

The authors also tried simulating the behavior of bubbles numerically. Spherical bubble motion and mutual interference with other bubbles are considered. We could only simulate the case that the distance between bubbles was far enough, because we assumed linear mutual interference among bubbles. The results showed that the central bubble near the wall collapsed later than the surrounding bubbles and produced the highest pressure. At that moment the surrounding bubbles started rebounding. This results correspond qualitatively to the experimental results described above. To investigate more realistic condition, nonlinear mutual interference and denser bubble distribution should be considered.

Acknowledgments

The authors would like to thank the following professors: Prof. Soyama at Tohoku University for his kindly offer of a piece of PVDF film and technical advice for our sensors, Prof. Takahira at Osaka Prefecture University for his technical advice for our numerical simulations, and Prof. Matsumoto at The University of Tokyo for his suggestion of the scenario of the collapse of cavitation bubble clusters. We also express our gratitude to Riken Denshi Co. Ltd. for their gratuitous remodeling of the transient converter to produce trigger output.

References

D'Agostino, L. and Brennen, C. E. (1989), *J. Fluid Mech.*, **199**, 155–176.

Kameda, M. and Matsumoto, Y. (1996), *Phys. Fluids*, **8** (2), 322–335.

Kumar, S. and Brennen, C. E. (1993), *J. Fluid Mech.*, **253**, 565–591.

Prosperetti, A. and Lezzi, A. (1986), *J. Fluid Mech.*, **168**, 457–478.

Sato, K. and Ogawa, N. (1995), *ASME FED*, **226**, 119–125.

Shimada, M., Kobayashi, T. and Matsumoto, Y. (1999), *Proc. of FEDSM'99*, FEDSM99-6775 (CD-ROM).

Shimada, M., Matsumoto, Y. and Kobayashi, T. (2000), *JSME Int. J, Ser. B*, **43** (2), 380–385.

Soyama, H., Lichtarowicz, A. and Momma, T. (1996), *ASME FED*, **236**, 415–422.

Stutz, B. and Reboud, J.-L. (1997a), *Exp. Fluids*, **22** (3), 191–198.

Stutz, B. and Reboud, J.-L. (1997b), *Phys. Fluids*, **9** (12), 3678–3686.

Stutz, B. and Reboud, J.-L. (2000), *Exp. Fluids*, **29** (6), 545–552.

Takahira, H., Akamatsu, T. and Fujikawa, S. (1994), *JSME Int. J., Ser. B*, **37** (2), 297–305.

Takahira, H., Yamane, S. and Akamatsu, T. (1995), *JSME Int. J., Ser. B*, **38** (3), 432–439.

Yamaguchi, H. and Kato, H. (1983), *2nd Int. Conf. on Cavitation*, 167–174.

Wang, Y. C. and Brennen, C. E. (1994), *ASME FED*, **194**, 15–19.

Wang, Y. C. and Brennen, C. E. (1995), *ASME FED*, **226**, 17–29.